

Copyright © 2009. Reprinted from APPLIED PHYSICS LETTERS. 93,022901.2008. Such permission of the American Institute of Physics does not in any way imply the American Institute of Physics endorsement of any of Institute of Microelectronics' products or services. Internal or personal use of this material is permitted. However, permission to reprint/republish this material for advertising or promotional purposes or for creating new collective works for resale or redistribution must be obtained from the American Institute of Physics by writing to [Rights@aip.org](mailto:Rights@aip.org).

## A nanoscale analysis of the leakage current in SiO<sub>2</sub> breakdown

Gang Zhang,<sup>1,a)</sup> Xiang Li,<sup>1,2</sup> Chih-Hang Tung,<sup>1</sup> Kin-Leong Pey,<sup>2</sup> and Guo-Qiang Lo<sup>1</sup>

<sup>1</sup>Institute of Microelectronics, Agency for Science, Technology and Research, 11 Science Park Road, Singapore 117685, Singapore

<sup>2</sup>School of Electrical and Electronic Engineering, Nanyang Technological University, 50 Nanyang Avenue, Singapore 639798, Singapore

(Received 8 May 2008; accepted 22 June 2008; published online 14 July 2008)

In this work, we provide a nanoscale scheme of the leakage current in SiO<sub>2</sub> breakdown. In combination with first-principles calculation, the leakage current is explored with the Landauer–Büttiker transport formula. Large leakage current is generated from the band gap states. The effect of oxygen vacancy is remarkable in the conduction band while almost negligible in the valence band. Our results predict that in a nanoscale metal oxide semiconductor (MOS) field-effect transistor, the leakage current in *p*-MOS devices is much smaller than that in *n*-MOS devices.

© 2008 American Institute of Physics. [DOI: 10.1063/1.2957657]

The metal oxide semiconductor field-effect transistor (MOSFET) is currently the device of choice for integrated circuits. A thermally grown oxide of silicon, silicon dioxide, forming the insulating layer between the control “gate” and the conducting “channel,” is considered as the heart of MOSFET.<sup>1–3</sup> Advanced silicon processing technology has allowed MOSFET to be scaled down to submicron dimensions, realizing incredible gains in performance. With the rapid scaling of MOS devices, a SiO<sub>2</sub> gate dielectric approaches a nanometer scale. The rapid scaling and material substitution raise the concern of device reliability issues. Dielectric breakdown may lead to the partial or total loss of the functionality of the transistor. This eventually degrades the overall performance and determines the lifetime of logical devices. When gate dielectric is subjected to either constant voltage or current stress, traps or defects will be gradually generated, and a conducting path is formed as the density of traps or defects reaches a critical value, and hence, gate dielectric breakdown occurs. Several dielectric breakdown models<sup>4</sup> have been proposed to interpret an observed phenomenon. However, most of the breakdown phenomena are studied from the electrical point of view; very few reports on the physical analysis of the breakdown phenomenon can be found. Until now, an atomistic mechanism of the leakage current is still lacking because of the complex nature of dielectric breakdown. Moreover, as the rapid scaling down of the gate dielectric to 1–2 nm thickness, a microscopic picture of dielectric breakdown is indispensable. In this work, combining the Landauer–Büttiker transport formula with first-principles calculations, we will provide a nanoscale scheme of the leakage current. Understanding the microscopic origin of the detrimental effects in gate dielectrics gives rise to the hope that guided modifications in the process may yield devices that can reliably be extended to smaller structures.

A large number of theoretical and experimental researches have reached a general consensus that the neutral oxygen vacancy (*V*<sub>O</sub>) is a good candidate to describe deficient centers in SiO<sub>2</sub> breakdown.<sup>5–8</sup> Since the short range order of amorphous SiO<sub>2</sub> is known to be very similar to that of  $\alpha$ -quartz,<sup>9</sup> the  $\alpha$ -quartz is used in this work. We used a

periodic supercell of  $2 \times 2 \times 1$  unit cells containing 36 atoms (12 Si atoms and 24 O atoms) to model crystalline  $\alpha$ -quartz. It is demonstrated that with a large supercell model, first-principles calculations are promising tools to investigate the geometrical and electronic structures of SiO<sub>2</sub>.<sup>9</sup> In order to study the effect of *V*<sub>O</sub> concentration, we remove one ( $1-V_{O}$ ) and two ( $2-V_{O}$ ) oxygen atoms from the Si—O—Si network in  $\alpha$ -quartz, as shown in Fig. 1. In the construction, we ensure that the Si atoms in the  $\equiv\text{Si—Si}\equiv$  bonds are not on the supercell boundary. Therefore in this  $2 \times 2 \times 1$  supercell, the maximum number of *V*<sub>O</sub> is 2. After the initial configurations were constructed, geometry optimizations were performed using all electron density functional theory (DFT) implemented in a DMOL<sup>3</sup> package.<sup>10</sup> The DFT calculations were performed using generalized gradient approximation with the functional parametrized by Perdew, Burke, and Ernzerhof (PBE),<sup>11</sup> and the double-numerical-polarization basis set that includes all occupied atomic orbitals plus a second set of valence atomic orbitals plus polarized *d*-valence orbitals was employed. It was shown that the PBE functional gives an electronic structure for a large set of tested molecules closer to the experimental values than any other method available in DMOL<sup>3</sup>.<sup>12</sup> Self-consistent field calcula-

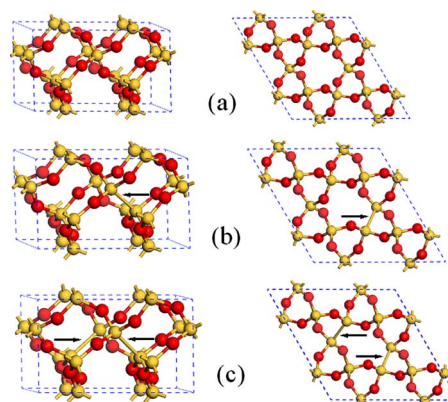


FIG. 1. (Color online) Schematic picture of the  $\alpha$ -quartz used in the calculation. Left column: side view; right column: top view. From up to down are undefected  $\alpha$ -quartz,  $1-V_{O}$   $\alpha$ -quartz, and  $2-V_{O}$   $\alpha$ -quartz. The blue dotted cage represents the  $2 \times 2 \times 1$  supercell volume. Si and O atoms are represented in yellow and red, respectively. The arrows indicate the *V*<sub>O</sub> centers.

<sup>a)</sup>Electronic mail: zhangg@ime.a-star.edu.sg.

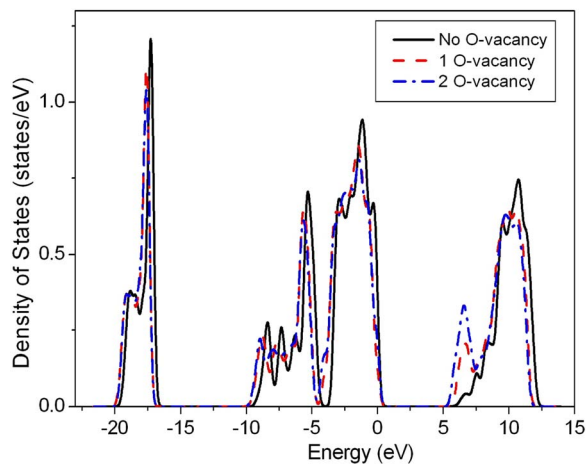


FIG. 2. (Color online) DOS for undefected  $\alpha$ -quartz,  $1-V_O$   $\alpha$ -quartz, and  $2-V_O$   $\alpha$ -quartz. The highest occupied states are aligned at 0 eV.

tions were done with a convergence criterion of  $10^{-6}$  hartree on the total energy. The Brillouin zone integration was performed using a  $6 \times 6 \times 6$  Monkhorst–Pack  $k$ -point grid. All the structures were fully optimized with a convergence criterion of 0.002 hartree/Å for the forces and 0.005 Å for the displacement. A real-space cutoff of 4.0 Å for the atom-centered basis set was chosen to increase computational efficiency while not significantly affecting the magnitude of interatomic forces or the total energies. The Gaussian smearing of electron density was applied with the energy range of 0.2 eV.

The equilibrium structures of  $\alpha$ -quartz and  $\text{SiO}_2$  with  $1-V_O$  and with  $2-V_O$  are shown in Fig. 1. To benchmark the computational method, preliminary calculation on the  $\alpha$ -quartz has been performed. Our predicted quartz structure exhibits Si—O bond lengths of 1.625 and 1.631 Å. The bond lengths are 1% longer than experiment<sup>13</sup> and agree with previous calculations<sup>14,15</sup> within 0.1%. Our bond angle is  $2^\circ$  smaller than experiment,<sup>13</sup> which results from the slight expansion in the bond lengths compared to experiment. The asymmetry between short and long bonds, 0.4%, is close to the experimental value of 0.5%.<sup>13</sup>

In the  $V_O$  center, an oxygen atom is removed and the silicon dangling bonds combine to form a direct silicon-silicon bond. Figures 1(b) and 1(c) show the relaxed configurations of  $1-V_O$  and  $2-V_O$  centers in  $\alpha$ -quartz. The formation of a  $V_O$  center results in a short  $d_{\text{Si-Si}}=2.44$  Å for  $1-V_O$  (2.46 Å for  $2-V_O$ ) due to the formation of a two-center, two-electron bond. The features of the local configurations are in good agreement with previous first-principles calculations,<sup>16</sup> providing support for the accuracy of the current model. It is interesting that the generation of the second  $V_O$  does not affect the local configuration of the first  $V_O$  and only increases the Si—Si bond length slightly. The calculated densities of states (DOSs) of  $\alpha$ -quartz, with  $1-V_O$  and with  $2-V_O$ , are shown in Fig. 2. Here the highest occupied states (valence band maximum) are aligned at 0 eV. In the total DOS of  $\alpha$ -quartz, one sees four distinct bands, the oxygen  $S$  states ( $-20$  to  $-16$  eV), the strong-bonding states ( $-9$  to  $-4$  eV), the lone-pair-like band ( $-3$  to 0 eV), and the weak-antibonding conduction states (6 eV and above). It should be noted that the calculated band gap of  $\alpha$ -quartz is 5.8 eV, which is substantially lower than the true band gap of about 9 eV. This magnitude of underestimation is typical of the

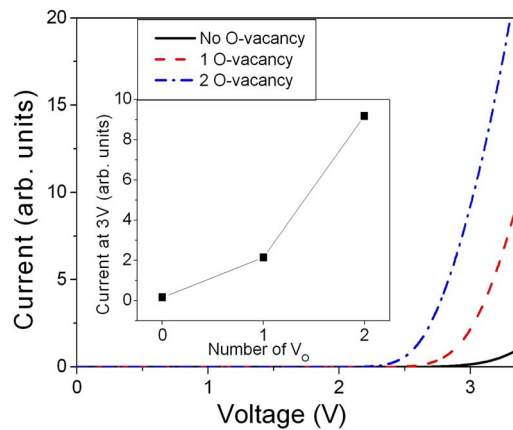


FIG. 3. (Color online) Leakage currents for  $\alpha$ -quartz,  $1-V_O$   $\alpha$ -quartz, and  $2-V_O$   $\alpha$ -quartz.

Kohn–Sham equations. At the  $V_O$  centers, from the combination of the  $sp^3$  hybrids on each Si, a doubly occupied  $\sigma$  bonding and an empty  $\sigma^*$  antibonding state appear in the band gap. The band gap state is contributed by the  $V_O$ . The effect of  $V_O$  is remarkable in the conduction band while almost negligible in the valence band. When the  $V_O$  concentration increases, the intensity of the defect state at the conduction band edge increases obviously, while the peak position changes slightly.

When a voltage is applied across the gate oxide, current will flow if the voltage is high enough. With the first-principles predicted DOS, we calculate the leakage current by the Landauer–Büttiker transport formula,

$$I(V) = \frac{4e}{h} \int D(E)[F(E - eV) - F(E)]dE. \quad (1)$$

Here  $D(E)$  is the DOS for electrons of energy  $E$ , and  $F(E)$  is the Fermi function for the electrode. Landauer–Büttiker transport formula have been used to study electron transport property in nanoscale.<sup>17</sup> Here only the lowest conduction band of the  $\text{SiO}_2$  contributes here, which corresponds to the current through  $n$ -type silicon and  $\text{SiO}_2$  system. The integration region covers the conduction band of  $\text{SiO}_2$ . Moreover the band offset (corresponding to the barrier height between  $n$ -type silicon and  $\text{SiO}_2$ ) is 3 eV. This value is the conduction band offset of  $\text{SiO}_2/\text{Si}$  for a typical MOSFET device. Within these approximations, the current versus voltage is shown in Fig. 3. For both undefected  $\text{SiO}_2$  and defected  $\text{SiO}_2$ , the current starts to increase with bias at about 3 V, but the values of the current are quite different. With  $V_O$  defect, the local leakage current increases remarkably. For instance, at 3 V bias, the leakage current in  $2-V_O$  and  $1-V_O$   $\text{SiO}_2$  are 60 times and 15 times of that in undefected  $\text{SiO}_2$ . These large leakage currents are contributed from the band gap states near the conduction band edge. When  $V_O$  defect concentration increases, the intensity of band gap states increases, thus inducing larger leakage currents. The microscopic calculated current is consistent with the idea that dielectric breakdown can be generally defined as the local increase in conductance.

In the  $\text{SiO}_2$  network, the effect of O vacancies is equivalent to a  $p$ -type doping (shown in Fig. 2). The lowered conduction band edge enhances the tunneling of carriers from adjacent electrodes, and the leakage current increases dramatically when a relatively large biasing voltage is applied.

In *p*-type devices, the current conduction is through a carrier hole that flows through the valence band edge; in *n*-type devices, the carrier is an electron that flows through the conduction band. From the negligible impact of  $V_O$  on the valence band edge, we can predict that there will be a small leakage current through the  $\text{SiO}_2$  valence band edge. In other words, in nanoscale MOSFET, when suffering from oxide breakdown, the leakage current in the *p*-MOS device is much smaller than that in the *n*-MOS device.

In this work, we provide a nanoscale scheme of the leakage current of the  $\text{SiO}_2$  breakdown with the combination of the Landauer–Büttiker transport formula with first-principles calculations. The  $\alpha$ -quartz configuration of  $\text{SiO}_2$  has been constructed by relaxation using the first-principles method. The oxygen deficient centers are formed by removing identical oxygen atoms from the Si—O—Si networks. A large leakage current is contributed from the band gap states, which are generated by the oxygen vacancies. The effect of  $V_O$  is remarkable in the conduction band while almost negligible in the valence band. We predict that in nanoscale MOSFET, when suffering from oxide breakdown, the leakage current in *p*-MOS devices is much smaller than that in *n*-MOS devices.

- <sup>1</sup>E. H. Nicollian and J. R. Brews, *MOS (Metal Oxide Semiconductor) Physics and Technology* (Wiley, New York, 1982).
- <sup>2</sup>G. Pacchioni, L. Skuja, and L. D. Griscom, *Defects in  $\text{SiO}_2$  and Related Dielectrics: Science and Technology* (Kluwer Academic, Dordrecht, The Netherlands, 2000).
- <sup>3</sup>R. A. B. Devine, J.-P. Duraud, and E. Dooryhee, *Structure and Imperfections in Amorphous and Crystalline Silicon Dioxide* (Wiley, New York, 2000).
- <sup>4</sup>S. Lombardo, J. H. Stathis, B. P. Linder, K. L. Pey, F. Palumbo, and C. H. Tung, *J. Appl. Phys.* **98**, 121301 (2005).
- <sup>5</sup>L. Skuja, *J. Non-Cryst. Solids* **239**, 16 (1998).
- <sup>6</sup>H. Imai, K. Arai, and H. Imagawa, *Phys. Rev. B* **38**, 12772 (1988).
- <sup>7</sup>D. L. Griscom and M. Cook, *J. Non-Cryst. Solids* **182**, 119 (1995).
- <sup>8</sup>S. Agnello, R. Boscaino, G. Buscarino, M. Cannas, and F. M. Gelardi, *Phys. Rev. B* **66**, 113201 (2002).
- <sup>9</sup>J. Sarnthein, A. Pasquarello, and R. Car, *Phys. Rev. Lett.* **74**, 4682 (1995).
- <sup>10</sup>DMOL is a density functional theory package distributed by Accelrys Inc; B. Delley, *J. Chem. Phys.* **92**, 508 (1990).
- <sup>11</sup>J. P. Perdew, K. Burke, and M. Ernzerhof, *Phys. Rev. Lett.* **77**, 3865 (1996).
- <sup>12</sup>G. Zhang and C. B. Musgrave, *J. Phys. Chem. A* **111**, 1554 (2007).
- <sup>13</sup>L. Levien, C. T. Prewitt, and D. J. Weidner, *Am. Mineral.* **65**, 920 (1980).
- <sup>14</sup>D. R. Hamann, *Phys. Rev. Lett.* **76**, 660 (1996).
- <sup>15</sup>P. E. Blochl, *Phys. Rev. B* **62**, 6158 (2000).
- <sup>16</sup>T. Tamura, G.-H. Lu, and R. Yamamoto, *Phys. Rev. B* **69**, 195204 (2004).
- <sup>17</sup>G. Zhang, Z.-L. Cao, and B.-L. Gu, *Mod. Phys. Lett. B* **14**, 717 (2000).